Measuring mechanodynamics in an unsupported epithelial monolayer grown at an air–water interface

Corinne Gullekson[a], Matthew Walker[b], James L. Harden[a,c], and Andrew E. Pelling[a,b,d,e,*]
[a]Centre for Interdisciplinary NanoPhysics, Department of Physics, [b]Department of Biology, [c]Ottawa Institute of Systems Biology, and [d]Institute for Science Society and Policy, University of Ottawa, Ottawa, ON K1N5N5, Canada; [e]SymbioticA, School of Anatomy, Physiology and Human Biology, University of Western Australia, Perth, WA 6009, Australia

ABSTRACT **Actomyosin contraction and relaxation in a monolayer is a fundamental biophysical process in development and homeostasis. Current methods used to characterize the mechanodynamics of monolayers often involve cells grown on solid supports such as glass or gels. The results of these studies are fundamentally influenced by these supporting structures. Here we describe a new method for measuring the mechanodynamics of epithelial monolayers by culturing cells at an air–liquid interface. These model monolayers are grown in the absence of any supporting structures, removing cell–substrate effects. This method's potential was evaluated by observing and quantifying the generation and release of internal stresses upon actomyosin contraction (800 ± 100 Pa) and relaxation (600 ± 100 Pa) in response to chemical treatments. Although unsupported monolayers exhibited clear major and minor strain axes, they were not correlated with nuclear alignment as observed when the monolayers were grown on soft deformable gels. It was also observed that both gels and glass substrates led to the promotion of long-range cell nuclei alignment not seen in the hanging-drop model. This new approach provides us with a picture of basal actomyosin mechanodynamics in a simplified system, allowing us to infer how the presence of a substrate affects contractility and long-range multicellular organization and dynamics.**

Monitoring Editor
Manuel Théry
CEA, Hopital Saint Louis

Received: May 16, 2016
Revised: Oct 11, 2016
Accepted: Nov 2, 2016

INTRODUCTION

Contractility is involved in the remodeling and organization of the cell interior and plays a major role in multicellular morphogenesis over long distances and time scales (Rauzi *et al.*, 2010; Harris *et al.*, 2012; Roh-Johnson and Shemer, 2012). There is increasing interest in understanding how contractility manifests in multicellular systems (Nelson *et al.*, 2005; Fernandez-Gonzalez *et al.*, 2009; Rauzi *et al.*, 2010). Contractile forces generated by the actomyosin cytoskeleton within individual cells collectively generate tissue-level forces (Vicente-Manzanares *et al.*, 2009; Martin *et al.*, 2010). A major challenge in developmental biology is to understand how cytoskeletal activity is orchestrated to produce higher-order tissue organization (Fernandez-Gonzalez *et al.*, 2009). Therefore understanding tissue morphogenesis requires determining how cellular forces are integrated across cells and tissues (Martin *et al.*, 2010).

Actomyosin contraction is one of the major sources of internal force inside of the cell. The actin cytoskeleton structure in epithelial monolayers is highly dependent on cell attachment. In epithelia, the cell–cell attachment points—adherens junctions—link a thick circumferential ring of actin and myosin around each cell that is aligned with the cell borders (Owaribe *et al.*, 1981; Yonemura *et al.*, 1995). The contractility of these marginal actin bundles is used for morphogenesis, facilitating epithelial sheet bending and invagination (Leptin, 2005; Lecuit and Lenne, 2007). The substrate attachment points—focal adhesions—link actin stress fibers. Cell contractility is commonly described and investigated in terms of changes in cortical cell elasticity as well as traction dynamics—the resistance of the substrate to deformation—on flexible substrates (Discher *et al.*, 2005;

This article was published online ahead of print in MBoC in Press (http://www.molbiolcell.org/cgi/doi/10.1091/mbc.E16-05-0300) on November 9, 2016.

*Address correspondence to: Andrew E. Pelling (a@pellinglab.net).

Abbreviations used: CalA, calyculin A; FBS, fetal bovine serum; GFP, green fluorescent protein; MDCK, Madine–Darby canine kidney; PA, polyacrylamide; PBS, phosphate-buffered saline; WGA, wheat germ agglutinin.

Rauzi *et al.*, 2008). Generally, changes in cortical cell elasticity and traction dynamics are linked to sensing of the mechanical microenvironment (Vogel and Sheetz, 2006; Trichet *et al.*, 2012). Traction dynamics is linked to cortical elasticity, focal adhesion organization, and cell morphology (Pelham and Wang, 1997; Discher *et al.*, 2005; Solon *et al.*, 2007). Often, fundamental studies of actomyosin contraction and relaxation are examined in situations in which cells are grown on, or embedded in, flexible substrates. (Discher *et al.*, 2005; Ghibaudo *et al.*, 2009; Huh *et al.*, 2010; Tremblay *et al.*, 2013). There is intense interest in understanding the interplay and feedback between the mechanical properties of such substrates and contractility (Trichet *et al.*, 2012). Although such studies typically use substrates with systematically altered mechanical properties, the substrate is always present. Therefore it is difficult to assess the intrinsic internal mechanical dynamics and properties of cells in the absence of a mechanically supporting surface.

There has been interest in intrinsic mechanical properties of substrate-free epithelial sheets (Harris *et al.*, 2012, 2013). Measurements of the elasticity and failure of monolayers suspended between two flexible rods provided valuable insights into the understanding of epithelial mechanics (Harris *et al.*, 2012, 2013). Of importance, the measurements yielded mechanical properties of the near substrate-free cell sheet. With tensile testing of the suspended cultured monolayers, it was determined that rupture of intercellular junctions occurs after doubling the monolayer in length with an average force approximately nine times larger than measured in pairs of isolated cells (Chu *et al.*, 2004; Harris *et al.*, 2012), demonstrating that epithelial organization leads to a strong enhancement in the integrity of the tissue. However, this suspended monolayer is still mechanically constrained at suspension points that provide an external form of confinement and prestress.

This raises the question of how cell contractility, the organization of the cell interior, and long-range structural remodeling altered in the absence of mechanically confining or supporting structures in a multicellular system. The objective of this study was to develop a new method to characterize actomyosin mechanodynamics in a multicellular system when no resistance is offered by the surroundings. Understanding these dynamics could provide us with a picture of basal actomyosin mechanodynamics in a simplified model multicellular system. This method will also allow us to indirectly infer how the presence of a substrate affects actomyosin contractility and long-range multicellular organization and dynamics.

Here we used an in vitro hanging-drop culture protocol. We created Madin–Darby canine kidney (MDCK) epithelial monolayer clusters at an air–water interface. Using laser scanning confocal microscopy, we used cell nuclei within the monolayer as fiduciary markers to determine the internal strain developed in the clusters during basal and chemically induced contractile changes. We validated our method using two alternate methods for tracking cell deformation: 1) tracking the cell membrane boundary of the cluster and 2) tracking cell boundaries marked with green fluorescent protein (GFP)–actin. Of importance, this new method for studying the mechanodynamics of unsupported epithelial sheets opens the door to several future research directions, including investigations of the apicobasal polarization, myosin distribution, and actin ordering in the unsupported monolayer. This approach allows one to observe the results of forces that are important for many processes that take place in development (Heisenberg and Bellaïche, 2013) and may advance the understanding of how those forces are transmitted to neighboring cells, and how they are integrated to trigger global changes in tissue shape. The results of this study might also be relevant to three-dimensional (3D) cell culture, where hard surfaces are not present.

RESULTS

Deformation of monolayer clusters on solid substrates

To examine the influence of a mechanically supporting substrate, we created monolayer clusters on hard glass substrates and soft polyacrylamide (PA) gels (Young's modulus, 4.8 kPa). These clusters naturally occur in MDCK cell culture at low confluence. The clusters on glass were fixed and stained for DNA, actin, and vinculin (Figure 1A). A strong actin signal was localized in the perimeter of the cluster. Similarly, the vinculin also localized around the cluster perimeter. When epithelial cells form a cluster on solid substrates, more cellular adhesions and force generation appear at the cluster perimeter (Notbohm *et al.*, 2012; Mertz *et al.*, 2013; Ng *et al.*, 2014). To induce cluster relaxation and contraction in the clusters, we used the agents blebbistatin and calyculin A (CalA). Blebbistatin is a myosin II inhibitor that inhibits contraction and disrupts contractile filament organization (Lemmon *et al.*, 2009). CalA is a phosphatase inhibitor that is well known to induce contraction (Fernandez-Gonzalez *et al.*, 2009; Lemmon *et al.*, 2009). Clusters on glass were live stained with Hoechst, and the nuclei were tracked with the addition of drugs in

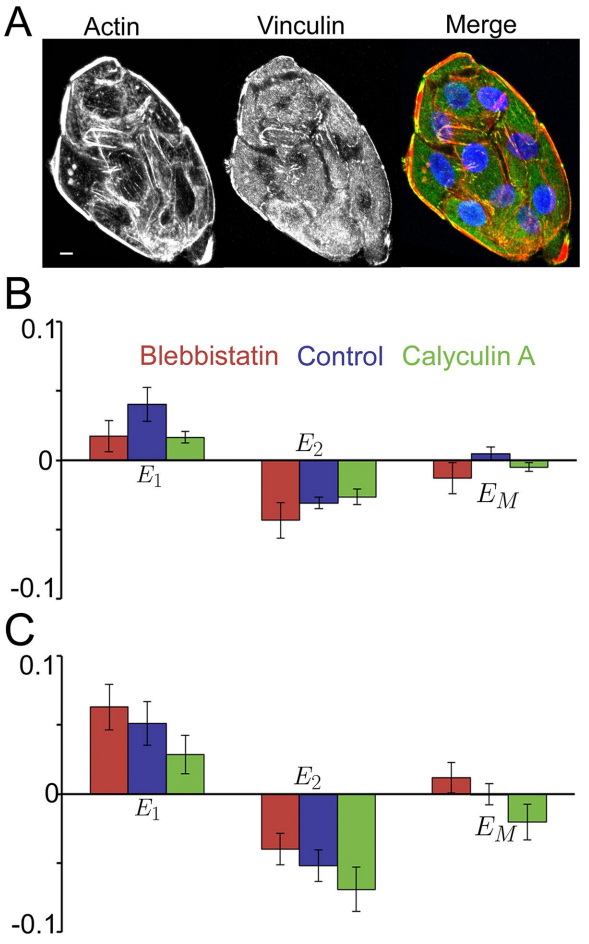

FIGURE 1: Deformation of the cluster on glass and PA. (A) Confocal actin (left), vinculin (middle), and merged (right; actin, red; vinculin, green; nucleus, blue) images of a cluster of MDCK cells on glass. (B) Major (E_1), minor (E_2), and mean (E_M) strains of cell clusters on glass after the addition of blebbistatin (red), medium (blue), or CalA (green). n = 11, 9, and 12, respectively; no significance. (C) Major (E_1), minor (E_2), and mean (E_M) strains of cell clusters on a PA gel after the addition of blebbistatin (red), medium (blue), or CalA (green). n = 15, 10, and 15, respectively; no significance. Bar, 10 μm.

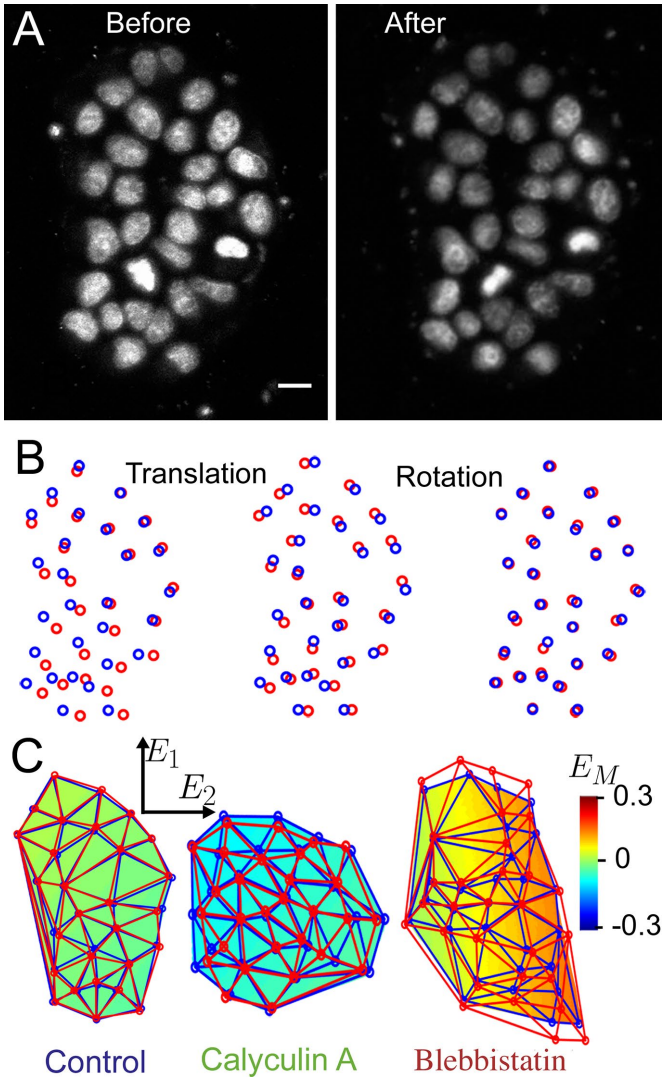

FIGURE 2: The process used to analyze the images. (A) Maximum intensity *Z*-projections of the before and after confocal images of cells in a hanging drop used for a control. (B) The positions of the nuclei in the before (blue) and after (red) images determined by threshholding. The raw nuclear positions (left) are shown, as well as the positions after the translation (middle) and after the rotation (right) of the after positions. (C) Positions of the before (blue) and after (red) nuclei in a mesh over a mean strain map of the cluster. The major and minor principal axes (E_1 and E_2) of the cluster are in the *y*- and *x*-directions, respectively. Maps are shown for the control (left) case, as well as for the CalA (middle) and blebbistatin (right) treatments in hanging drops. Bar, 10 μm.

order to determine strain in the cluster. This process is described in *Materials and Methods* and demonstrated with images of monolayer clusters grown in hanging drops (Figure 2). There was no significant difference in the mean strains of the clusters on glass with the different drug treatments ($p > 0.12$; Figure 1B). To investigate the deformation on a softer substrate, clusters were cultured on PA gels. Consistent with the glass substrates, there was no significant difference in the mean strains of the clusters on the gels with the different drug treatments ($p > 0.07$; Figure 1C). To examine more thoroughly the intrinsic deformation of a contracting or relaxing monolayer, the solid substrate should be removed, which is why the hanging-drop method was introduced.

Formation of a cell monolayer cluster

As MDCK cells migrate and proliferate in two-dimensional culture, the cells form islands that eventually merge to form a continuous monolayer (Zegers *et al.*, 2003). In 3D culture, individual MDCK cells plated within an extracellular matrix gel assemble into a hollow sphere that is lined by a monolayer of polarized epithelial cells (Zegers *et al.*, 2003). However, after incubation in a hanging drop, MDCK cells will form monolayer clusters of cells (Tchao, 1989; Eckhart *et al.*, 2003; Inoue *et al.*, 2005). This is in contrast to mesenchymal stem cells, which gradually coalesce into a single central spheroid along the lower surface of the drop (Bartosh, 2010). MDCK cells in a hanging drop will form a basement membrane–like sheet of cell-secreted proteins, providing the matrix for the proliferating cells (Eckhart *et al.*, 2003; Inoue *et al.*, 2005). Previous immunohistochemical studies demonstrated the presence of type IV collagen, laminin 1, and laminin 5 in the membrane, and enzyme digestion experiments indicated that this membrane was sensitive to collagenase (Eckhart *et al.*, 2003). In previous studies, it was shown that the tension carried by basement membranes is modest compared with the tension carried by the cellular portion of the epithelium (Wiebe *et al.*, 2005) and that the basement membrane is thinner and softer than the cellular component, with a Young's modulus of 7.5 kPa (Last *et al.*, 2009) compared with 20 kPa (Harris *et al.*, 2012). Moreover, this basement membrane is relatively free to move along the air–water interface. Therefore this basement membrane–like sheet allows cells to form healthy monolayers while still being relatively unrestrictive to collective cellular deformation.

Epithelial monolayer clusters were grown in these hanging drops, and their nuclei were used to track deformations during changes in contractility. The clusters were similar in number of cells (average of 23 ± 2 cells/cluster) to the ones used in the solid-substrate experiments (average of 21 ± 2 cells/cluster). To label cell nuclei, we added the common nuclear stain Hoechst 33342 to the drop with a pipette in the lid's inverted state (Figure 3, A and B). In all cases, 1 μl of a stock solution of blebbistatin, CalA, or medium (control) was added to the hanging drop for 30 min in a cell culture incubator. The nuclei of suspended clusters were imaged before and after the addition of the drugs or control. On average, only five monolayer clusters formed in each hanging drop and it was straightforward to image the same cluster before and after the 1-μl addition.

Hanging-drop shape

The shape of the droplet observed in this setup can be approximated as a spherical cap (Figure 3C). The radius, *r*, at the droplet's top, where it is attached to the dish lid, was measured optically at 2.9 ± 0.1 mm ($n = 7$). The droplet volumes were measured using the mass of the droplets to be 39.49 ± 0.04, 40.29 ± 0.06 after Hoechst addition, and 41.18 ± 0.07 μl after drug addition ($n = 10$). Using the spherical cap model, we calculated the height, *h*, and radius of curvature, *R*, of the initial droplet to be 2.5 ± 0.1 and 2.9 ± 0.1 mm, respectively. With the addition of 2 μl, the height of the droplet increased by 74.4 ± 0.5 μm, and the radius of curvature decreased by 14 ± 8 μm (0.5% decrease). The average diameter of clusters was ~150 μm. With the comparatively large radius of curvature, the center and edge of the cluster had a height difference of only 0.96 ± 0.04 μm. For this reason, it was reasonable to approximate the curved bottom of the drop as a flat surface. Owing to the small size of the droplet, scans were acquired quickly to avoid evaporation effects. Under the imaging power used in this study, some evaporation of the droplet did occur, resulting in a height decrease of 0.24 ± 0.02 μm/s, which corresponds to a

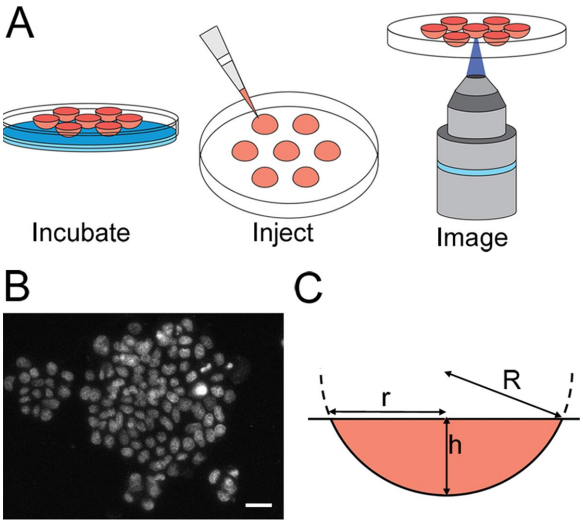

FIGURE 3: Experimental protocol used to create monolayer clusters in hanging drops. (A) The process used to grow, stain, and image the monolayer clusters before and after the addition of cytoskeletal drugs. The 40-µl droplets were incubated overnight with PBS in the bottom of the dish. The dish lid was flipped, and 1 µl of Hoechst stain in medium was added with a pipette. The droplets were then imaged with a confocal microscope. After this, drugs were added to the droplets, which were incubated for 30 min and imaged again. (B) A typical set of clusters found in a droplet after the addition of Hoechst stain. (C) Diagram describing the shape of the droplet, which can be approximated as a spherical cap with a radius of curvature R. The radius at the droplet's top, r, is 2.9 ± 0.1 mm. The approximate height of the droplet, h, is calculated with the known volume of the droplet, $V = \frac{1}{6}\pi h(3r^2 + h^2)$. Bar, 20 µm.

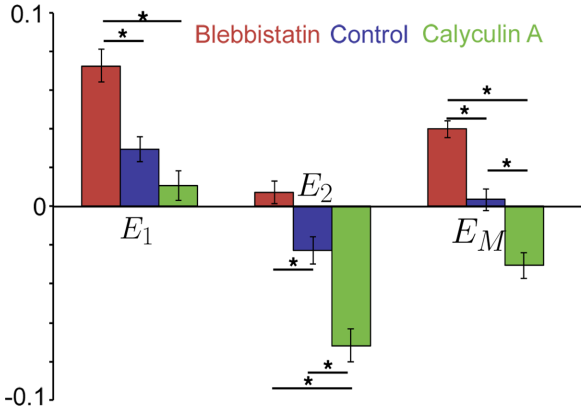

FIGURE 4: Deformation of the clusters in hanging drops with cytoskeletal drugs. Major (E_1), minor (E_2), and mean (E_M) strains of cell clusters after the addition of blebbistatin (red), medium (blue), or CalA (green). $n = 22$, $p < 0.05$.

change in volume of 0.32 ± 0.02 µl/min (Supplemental Figure S1). For this reason, image collection was always maintained <45 s. The radius of curvature only decreased by a maximum of 1.5 ± 0.1 µm during imaging, having little effect on the curvature of the monolayer clusters (<0.05%).

Deformation of monolayer clusters in hanging drops

The cytoskeletal drugs blebbistatin and CalA were used to relax and contract the cell clusters. The displacements of the cell nuclei were fitted to determine the major and minor principal strains (E_1 and E_2) of the cluster. As a control, 1 µl of medium was added to the drops, followed by incubation for 30 min between imaging. We did observe slight movement of nuclei within the cluster. However, the mean strain of the clusters in the control study was not significantly different from zero ($p > 0.89$; Figure 4). As expected, there was no significant dilation or contraction. The myosin II inhibitor blebbistatin caused clusters to dilate appreciably. The mean strain was significantly higher ($p < 0.00001$) than the control. Clusters also contracted with the addition of CalA, resulting in a mean strain that was significantly lower ($p < 0.0004$) than the control (Figure 4).

Cluster outline deformation

To determine whether the perimeter of the monolayer cluster itself deforms in a manner consistent with the changes in nuclei position, we tracked the cluster outline by fluorescently labeling cell membranes with wheat germ agglutinin (WGA). Tracking points on the cluster perimeter allowed us to determine monolayer strain (Supplemental Figure S2A). The major and minor strains in the cluster were calculated from nuclei positions, as well as from its outline. The strains calculated using cell nuclei and cluster outlines were not significantly different for the untreated control ($p > 0.90$), blebbistatin ($p > 0.85$), and CalA treatments ($p > 0.82$; Supplemental Figure S2B). This suggests that the contraction and relaxation observed in the nuclear positions are good indicators of total cluster deformation.

Individual cellular strains

To determine individual cellular strains during cluster contraction and relaxation, we used cells transiently expressing actin-GFP to form suspended clusters. We found that when a high percentage of cells were expressing actin-GFP, CalA treatments had no effect on contraction. Therefore we adjusted the transfection efficiency to ~25% of cells in order to create suspended clusters that exhibited the same mechanical dynamics as nontransfected cells. In this case, we felt confident that we would be able to examine individual cellular strains, albeit only on a subpopulation of cells within each cluster. Distinct actin stress fibers were not evident, but actin was found localized to the cell margins, allowing us to easily determine cell boundaries (Figure 5, A and B). Experiments with blebbistatin, CalA, and control conditions were performed once again, and nuclei positions were tracked, as well as the deformation of single cells within the cluster.

In the control, the cluster underwent normal basal remodeling, as seen by nuclear displacements. With the addition of CalA and blebbistatin, the nuclear displacements showed contraction and relaxation of the cluster, as expected (Figure 5C). The means of the strains in the individual cells were not significantly different from the cluster strains calculated by nuclear displacements in the control ($p > 0.97$), blebbistatin ($p > 0.96$), and CalA treatments ($p > 0.98$). This demonstrates that the monolayer cluster strains determined by nuclei correspond well to the deformation of the individual cells themselves.

Substrate effects on strain

Comparing the blebbistatin- or CalA-induced strains on the glass or PA substrates to the hanging drop (Figure 6A) reveals that they were significantly muted ($p < 0.002$ in both cases on glass, and $p < 0.04$ for blebbistatin on PA) by the substrate. Of interest, however, there was no significant difference in the controls ($p > 0.87$).

Feature orientation

To determine whether the deformation of the cluster exhibited a dependence on structural features of the cells, we calculated nematic

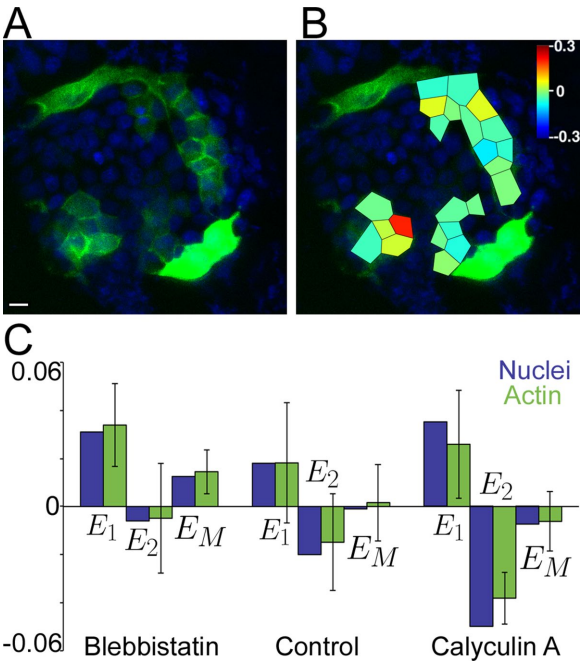

FIGURE 5: Cellular deformations inside a deforming hanging-drop cluster. (A) The before image of a MDCK cluster stained with Hoechst stain (blue) partially transduced with GFP-actin (green). (B) The mean strain of each cell overlaid on the before image. (C) Major, minor, and mean strain, of cell clusters after the addition of blebbistatin, medium, or CalA (blue) compared with the strains in the individual cells as calculated with the actin cell boundaries (green). Bar, 10 μm.

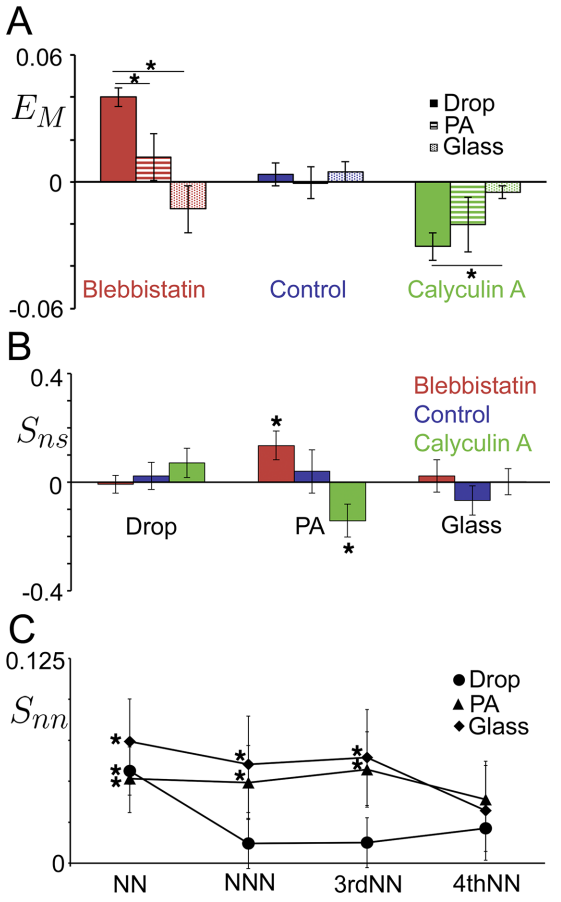

FIGURE 6: Substrate dependence on nuclear deformation. (A) Mean E_M strains of cell clusters in hanging drops (solid; $n = 22$), on PA gels (stripes; $n = 15$, 10, and 15), and on glass (dots; $n = 11$, 9, and 12) after the addition of blebbistatin (red), medium (blue), or CalA (green). (B) Order parameter S_{ns} for nuclei (defined by the angle between the major strain axis and the nuclear major axis) for blebbistatin (red), control (blue), and CalA (green) treatments for hanging drops, PA, and glass. (C) Order parameter S_{nn} for nuclei (defined by the angle between the nuclear major axis and its neighbor's nuclear major axis) in hanging drops (circles), on PA (triangles), and on glass (diamonds). The results are shown for nearest, next-nearest, third-nearest, and fourth-nearest neighbors. $p < 0.05$.

order parameters as described in *Materials and Methods*. The order parameter for nuclear alignment with strain (S_{ns}) was calculated for all the clusters (Figure 6B). The order parameters in the hanging drops were not significantly different from 0 ($p > 0.82$, 0.64, and 0.20 for blebbistatin, control, and CalA, respectively), suggesting no preferential alignment. On glass, the order parameters were also not significantly different from 0 ($p > 0.71$, 0.25, and 0.97 for blebbistatin, control, and CalA, respectively), suggesting no preferential alignment. However, since the strains were small on glass, the major strain axis was likely determined by basal remodeling of the cells and not the contraction or relaxation of the actomyosin cytoskeleton. On PA, the control order parameter was not significantly different from 0 ($p > 0.62$); however, the order parameters of nuclei of treated clusters were significantly different from 0. In the blebbistatin-treated clusters, the nuclei preferentially aligned with the major strain axis ($p < 0.04$). In the CalA-treated clusters, the nuclei preferentially aligned with the minor strain axis ($p < 0.04$). Therefore the nuclei tended to be aligned with the relaxation and contraction axes. This demonstrated that there was a correlation between nuclear alignment and cluster strain on PA gels that was not observed in hanging drops or on rigid glass substrates.

The order parameter S_{ls}, calculated with the angle between the major length axis and the major strain axis of the cluster (Supplemental Figure S3A), was not significantly >0 for any treatment or substrate ($p > 0.09$ in all cases). Another order parameter (S_{nl}) examines whether the nuclei were aligned with the major length axis on the cluster. Again, this parameter was not significantly >0 for any treatment or substrate ($p > 0.57$ in all cases; Supplemental Figure S3B). The average eccentricities of the nuclei grown on the three different substrates were not significantly different ($p > 0.15$). The clusters also had varying major/minor length aspect ratios; however, the mean strains observed in the monolayer clusters did not display any correlation with aspect ratio (Supplemental Figure S4).

To examine the alignment of cells with their neighbors, the order parameters between nuclei (S_{nn}) were calculated (Figure 5D). For all substrates, the order parameters for the nearest neighbors were significantly >0 ($p < 0.002$, 0.02, and 0.005 for hanging drops, PA, and glass, respectively), suggesting a local alignment of cells in direct contact. For next-nearest neighbors and third-nearest neighbors, the order parameter was not significantly >0 for hanging drops ($p > 0.4$ and 0.4, respectively) but was significantly >0 for PA ($p < 0.03$ and 0.02) and glass ($p < 0.05$ and 0.03). Beyond third-nearest neighbors, the order parameters were not significantly different from 0 in any case. This suggests that the cells on substrates aligned with cells that were near them even if they were not in direct contact. Of interest, this was not seen for cells in hanging drops, suggesting that longer-range cell alignment occurs only in monolayer clusters on solid substrates.

DISCUSSION

Understanding actomyosin contractility is one key aspect of cell mechanics that is required for explaining the dynamics of tissue remodeling. Direct experimental measurements of force generation in monolayer clusters without a rigid surface can aid in our understanding of the remodeling of epithelial monolayers. The objective of this study was to develop a new experimental method and analysis framework for understanding the mechanodynamics of unsupported epithelial monolayers. The lack of a solid support provided a less complicated system that allowed for remodeling not possible on a solid substrate. This method also provides a rational approach to teasing apart substrate and intercellular connections.

As a validation of the practicality of the hanging-drop model, we investigated the effect of cytoskeletal drugs on the deformation of MDCK monolayer clusters in both the absence and presence of mechanically supporting substrates. By comparing cell response in these two support regimes, we were able to identify the intrinsic contractile dynamics of an epithelial monolayer cluster. We did not directly observe significant strain in the monolayer when grown on PA gels or glass. PA gels can deform enough to make it possible to measure traction forces in monolayers indirectly with the displacements of embedded beads in the substrate (Trepat *et al.*, 2009; Tambe *et al.*, 2011). Although it is enticing to relate previous traction measurements on monolayers to our nuclear strain data, it is not immediately clear whether there should be a relationship. The methodologies used in these approaches are highly distinct and unlikely to be probing identical aspects. Tractions are caused by cytoskeletal dynamics coupled to the substrate (Cai *et al.*, 2006; Kumar *et al.*, 2006), whereas nuclear displacements are caused by numerous factors that may not be directly linked to traction dynamics (Reinsch and Gönczy, 1998; Dupin and Etienne-Manneville, 2011). However, future combined traction force microscopy and nuclear displacement traction experiments could be performed to further probe this phenomenon. The deformation we observed by tracking nuclei in hanging-drop monolayers was echoed in the deformation of individual cell and monolayer cluster outlines. This verified the use of nuclei as an effective cluster deformation marker. The observed deformations established that the contraction and dilation of monolayer clusters could be directly observed in the absence of a substrate by tracking cell nuclei in hanging-drop clusters.

To calculate stress in our droplets, we used the mean strains obtained from our data and a Young's modulus for MDCK monolayers of 20 ± 2 kPa (Harris *et al.*, 2012). This results in an apparent decrease of stress of 800 ± 100 Pa for the blebbistatin treatment and an apparent increase of stress of 600 ± 100Pa for the CalA treatment. There was a negligible change in stress for the control case. In other experiments, MDCK cells grown on pillars have average traction stresses of ~800 Pa in a monolayer (Roure *et al.*, 2005). This demonstrates that the hanging-drop system can be used to calculate the intrinsic stress produced by actomyosin contraction and relaxation in monolayer clusters.

Furthermore, varying the cluster substrate allowed us to relate contractile dynamics to substrate rigidity. Our hanging-drop method allowed us to measure the intrinsic remodeling that can occur in response to actomyosin dynamics. This remodeling was muted by the presence of a solid substrate, demonstrating that cluster contraction is significantly restrained when bound to a rigid surface. In general, stiff substrates increase cell–substratum adhesion (Pelham, 1998; Engler *et al.*, 2004; Yeung *et al.*, 2005; Ghibaudo *et al.*, 2008) and increase traction forces (Maruthamuthu, 2011). It has also been shown that compliant substrates promote focal adhesions that are dynamic and irregular in shape, whereas stiff substrates promote the formation of stable arrays of elongated focal adhesions (Pelham, 1998). When the cells are grown on glass, a large portion of the work from the actomyosin contraction is converted into substrate deformation instead of cellular remodeling. On softer substrates (PA gels in particular), cells are still restrained, but the smaller, more dynamic focal adhesions may allow for more movement. In this case, a smaller portion of the work will go into deforming the substrate. The contraction energy of the hanging-drop cells is expected to be smaller than the contraction energy of cells on glass or PA. However, the cells can move more freely in the cluster because they are not attached by focal adhesions to a substrate that is difficult to deform. Only a negligible amount of work should go into deforming the basement membrane–like sheet below the monolayer cluster, allowing for the larger cellular remodeling events observed in this study.

Of interest, when the clusters were grown on PA gels, there was a correlation between major strain direction and nuclear alignment. However, for cells grown on at the air–water interface in a hanging drop, the direction of the major strain was independent of nuclear alignment. The nuclei of single epithelial cells grown on flat, rigid surfaces were previously found to align with the actin cytoskeleton and the major length axis of the cell (McKee *et al.*, 2011; Raghunathan *et al.*, 2013). This suggests that the actin fibers are aligned with the major strain direction when on PA gels. This is congruous with the theory that individual cells contract and relax preferentially in the direction of their actin cytoskeletons, resulting in a global deformation along the cluster axis with which many cells are aligned. It was shown that matrix stiffness aids in regulating the polarization and alignment of stress fibers within cells (Zemel *et al.*, 2010). The lack of correlation between nuclear orientation and strain in the hanging drop may be due to reduced alignment of actin within each cell and the reduction in longer-range correlated cell–cell alignment observed on rigid substrates. In the case of the stiff glass substrate, although there should be greater alignment due to the substrate, focal adhesions pinned cells to the substrate, leading to null cluster strains and making it arduous to correlate to strain. The softer PA substrate allowed for substrate-mediated alignment and limited cell movement, permitting a correlation between cluster strain and nuclear alignment to be observed.

Remarkably, a solid substrate appears to be required for longer-range cell–cell alignment. By calculating nuclear order parameters, we found that cells in hanging drops were aligned only with their nearest neighbors, whereas cells on substrates were aligned with their next-nearest and third-nearest neighbors as well. This longer-range organization may be a result of substrate cues not present in hanging drops. It suggests also that signaling is necessary to develop long-range stresses. One possibility is that long-range orientational correlations are the result of elastic coupling of cells mediated by deformation of the compliant substrate. This is congruent with work showing that intercellular forces develop within the cluster of cells grown on a gel (Mertz *et al.*, 2013). This is also consistent with long-range correlations of substrate deformations and cell velocities previously observed in monolayers grown on PA gels (Angelini *et al.*, 2010). When low-density monolayers were examined on PA gels, velocity correlations were observed up to five cell lengths, as well as substrate deformation correlations up to four cell lengths. This deformation correlation length is only 25% longer than our nuclear orientation correlation length. This unexpected finding was made evident by comparison with the extreme condition of an air–water interface substrate. It would not have been possible without the novel hanging-drop monolayer. Our new method offers some surprising and novel insights into the mechanodynamics of epithelial

monolayers. However, it also raises several new questions that warrant further study.

For instance, do the cells in the monolayer establish apicobasal polarization? Is this polarization triggered without a solid substrate? This could be determined with more advanced staining techniques. Are the same structures formed on planar nonadhesive substrates, or is the curved drop shape needed? Plating cells in dishes with nonadhesive coatings could be a method to investigate this. How do clusters grown on substrates recoil when detached? This could be investigated using trypsin to detach the clusters from the substrate or by using thermosensitive polyacrylamide derivatives to allow release of the sheets. Future work will include computational modeling of these scenarios to examine these effects in further detail. These hanging-drop monolayers can also be made with epithelial cells stably expressing a fluorescently marked protein of interest and could also be used for a broad range of mechanical experiments investigating substrate effects on monolayers. Novel tools and methodologies for understanding the mechanics of monolayers will enable advances in biophysics.

There are many studies that systematically alter substrate elasticity to determine how the properties of a solid support regulate cell biology and biophysics. However, there is also the potential for a great deal more to be learned if the supporting substrate is removed entirely. This results in the loss of cell–substrate interactions, leaving cell–cell interactions to bear a greater role in regulating the system. We found that even in the absence of a solid substrate, there are still controlled mechanical responses to cytoskeletal drugs. By comparing the hanging-drop monolayers to monolayers on substrates, we found that a solid substrate is needed for higher-order alignments. This study establishes a new method. It is unclear what else can be discovered with it, and its ultimate effect will only be shown in time.

MATERIALS AND METHODS

Cell culture

MDCK epithelial cells were cultured in DMEM with 10% fetal bovine serum (FBS), 50 mg/ml streptomycin, and 50 U/ml penicillin antibiotics (all from Hyclone Laboratories, Logan, UT). Cells were cultured at 37°C in a 5% CO_2 incubator on 100-mm tissue culture dishes (Corning, Corning, NY). In some experiments, cells were cultured on solid substrates. In these cases, 1×10^5 cells were cultured in 34-mm tissue culture dishes (TPP, Trasadingen, Switzerland). The dishes contained either a flexible (soft) PA hydrogel coating, previously described (Wang *et al.*, 2000; Kandow *et al.*, 2007; Tse and Engler, 2010), or a bare glass coverslip bottom. To produce a PA gel with a Young's modulus of 4.8 kPa (Quinlan and Billiar, 2012), 7.5% acrylamide was polymerized with 0.053% bisacrylamide, 1 mg/ml ammonium persulfate (Bio-Rad, Hercules, CA), and 0.15% tetramethylethylenediamine (Bio-Rad) on (3-aminopropyl)trimethoxysilane (Sigma-Aldrich, St. Louis, MO)–coated coverslips. Before cell seeding, the hydrogel surface was functionalized with 100 µg/ml collagen (Life Technologies, Carlsbad, CA) in phosphate-buffered saline (PBS) using 0.5 mg/ml sulfo-SANPAH (Pierce, Waltham, MA) as a cross-linker. In some experiments, cells were cultured in hanging drops. MDCK cells were trypsinized and then resuspended in medium at a low dilution of 4000 cells/ml. The cells were then placed in hanging drops of 40 µl on the lower surface of the lids of plastic Petri dishes containing PBS. Hanging drops were imaged after 24 h of culture.

Drug treatments

Cells were treated with blebbistatin (Sigma-Aldrich) dissolved in dimethyl sulfoxide at a final concentration of 40 µM or calyculin A (Sigma-Aldrich) dissolved in water at a final concentration of 300 nM for 30 min in an incubator at 37°C and 5% CO_2 between before and after images.

Imaging

All images were acquired on a TiE A1-R laser scanning confocal microscope (LSCM; Nikon, Tokyo, Japan) with a 40× long working distance objective. Images were acquired with a standard LSCM configuration with appropriate laser lines and filter blocks. Cell nuclei were stained with Hoechst stain. In some cases, cells expressing GFP-actin were produced with BacMam reagent (CellLight Reagent BacMam 2.0; Invitrogen, Carlsbad, CA), using the manufacturer's protocols, at 20 particles/cell. Cells were plated and incubated for at least 48 h before being placed into hanging drops using the foregoing protocol. Cells were also stained with WGA coupled to Texas Red-X (Invitrogen) to reveal the cell membrane. Cells stained on glass were fixed with 3.5% paraformaldehyde and permeabilized with Triton X-100 at 37°C. Actin was stained with phalloidin–Alexa Fluor 546 (Invitrogen). Subsequently, this vinculin was stained with monoclonal anti-vinculin primary antibody (Sigma-Aldrich) and Alexa Fluor 488 rabbit anti-mouse immunoglobulin (Invitrogen) secondary antibody. DNA was labeled with 4′,6-diamidino-2-phenylindole (Invitrogen).

Strain quantification

The strain in the monolayer was determined with the displacements of the cell nuclei during a 30-min treatment. This method was validated by tracking the cell membrane boundary of the cluster and tracking actin in the cell margins. Images were processed and analyzed with ImageJ. Maximum intensity *z*-projections of 10, 5-µm-thick slices were used for strain calculations with no enhancements applied (Figure 2A). The positions of the nuclei in these images were determined using the analyze particles function after thresholding. The positions of the nuclei in the before and after images were manually linked and analyzed using Matlab. A Matlab program was used to account for differences in dish placement in the before and after images, as well as to determine nuclear displacements and calculate the strain tensor of the cluster.

In this program, nuclei positions were translated in both images so that the center of the nuclei was at the origin. These translated positions were then rotated so that the sum of the nuclei displacements was minimized (Figure 1B). This process was needed so that there were no artificially large displacements from the movement of the dish to and from an incubator between images. The initial positions (x, y) and displacements (u, v) of the nuclei were then used to fit the cluster with least squares to the displacement equations: $u = c_1x + c_2y + c_3xy + c_4x^2 + c_5y^2$ and $v = c_6x + c_7y + c_8xy + c_9x^2 + c_{10}y^2$ (Bathe, 2006). Second-order terms were included to account for nonconstant strain throughout the cluster. These equations were then used to determine the diagonal components of the Green–Lagrangian strain tensor (Rees, 2012),

$$E_{xx} = \frac{1}{2}\left(2\frac{\partial u}{\partial x} + \frac{\partial u}{\partial x}\frac{\partial u}{\partial x} + \frac{\partial v}{\partial x}\frac{\partial v}{\partial x}\right)$$

$$E_{yy} = \frac{1}{2}\left(2\frac{\partial v}{\partial y} + \frac{\partial u}{\partial y}\frac{\partial u}{\partial y} + \frac{\partial v}{\partial y}\frac{\partial v}{\partial y}\right)$$

Substitution of the displacement equations results in

$$E_{xx} = \frac{1}{2}(2(c_1 + c_3y + 2c_4x) + (c_1 + c_3y + 2c_4x)^2 + (c_6 + c_8y + 2c_9x)^2)$$

$$E_{yy} = \frac{1}{2}\left(2(c_7 + 2c_{10}y + c_8x) + (c_2 + 2c_5y + c_3x)^2 + (c_7 + 2c_{10}y + c_8x)^2\right)$$

These were used along with the shape of the cluster to determine the average *x*-axis extensional strain, E_{xx}, and average *y*-axis extensional strain, E_{yy}, in the cluster. The cluster was then rotated to find the principal axes by maximizing the difference between the *y*-axis strain and the *x*-axis strain. After this rotation, the *y*-axis strain was the major principal strain (E_1) and the *x*-axis strain was the minor principal strain (E_2; Figure 1C). The mean of the principal strains, $E_M = \frac{E_1 + E_2}{2}$, is the deformation due to a change in area (Mase *et al.*, 2009).

For experiments measuring the deformation of the cluster outline, points along the cluster outline labeled in the cell membrane–stained images were tracked and used in the foregoing code in place of nuclei positions. In some experiments, cellular-level strains were determined in cells expressing actin-GFP. Cell deformation was determined by fitting cell boundaries with polygons. The displacements of the vertices were least squares fitted to the displacement equations, $u = c_1x + c_2y$ and $v = c_3x + c_4y$, to impose uniform strain inside the cell (Bathe, 2006). Only first-order terms in the displacements *u* and *v* were required for these calculations because the individual cells were much smaller than the cluster. The strain in each cell was calculated using the principal strain axes of the cluster determined using the nuclei displacements.

Order parameter calculations

Orientational order parameters were calculated using the angles between different cluster features. The nematic order parameter was used, which in two dimensions is $S = \langle 2\cos^2\theta - 1 \rangle$ (Mercurieva and Birshtein, 1992). The order parameter will be 1 if the features are completely aligned, −1 if they are completely antialigned, and 0 if there is no alignment. The nuclei in the thresholded before images were fitted to ellipses in Matlab to determine the orientations of the major length axes and the eccentricities of the nuclei. The orientation of the major length axis of the cluster was determined by using the positions of the nuclei and finding the axis that minimized the square of the distances between the axis and the nuclei. Four different types of order parameters were calculated. Nuclei-strain order parameters (S_{ns}) were determined using the angles between the major length axes of the nuclei and the major strain axis of the cluster. Nuclei–cluster orientation order parameters (S_{nl}) were calculated using the angles between the major length axes of the nuclei and the cluster major length axis. Cluster orientation–strain order parameters (S_{ls}) were also calculated with the angles between the major length and major strain axes of clusters. In addition, nuclei–nuclei order parameters (S_{nn}) were calculated using the angles formed between the major axis of each nucleus and the major axis of its nearest neighbor. This was repeated for next-nearest, third-nearest, and fourth-nearest neighbors.

ACKNOWLEDGMENTS

This work was supported by a Natural Sciences and Engineering Research Council Discovery Grant. C.G. was supported by the uOttawa NSERC-CREATE program in Quantitative Biomedicine. A.E.P. gratefully acknowledges generous support from the Canada Research Chairs Program.

REFERENCES

Angelini TE, Hannezo E, Trepat X, Fredberg JJ, Weitz DA (2010). Cell migration driven by cooperative substrate deformation patterns. Phys Rev Lett 104, 168104.

Bartosh T (2010). Aggregation of human mesenchymal stromal cells (MSCs) into 3D spheroids enhances their antiinflammatory properties. Proc Natl Acad Sci USA 107, 13724–13729.

Bathe K-J (2006). Finite Element Procedures, Upper Saddle River, NJ: Prentice-Hall.

Cai Y, Biais N, Giannone G, Tanase M, Jiang G, Hofman JM, Wiggins CH, Silberzan P, Buguin A, Ladoux B, Sheetz MP (2006). Nonmuscle myosin IIA-dependent force inhibits cell spreading and drives F-actin flow. Biophys J 91, 3907–3920.

Chu Y-S, Thomas WA, Eder O, Pincet F, Perez E, Thiery JP, Dufour S (2004). Force measurements in E-cadherin-mediated cell doublets reveal rapid adhesion strengthened by actin cytoskeleton remodeling through Rac and Cdc42. J Cell Biol 167, 1183–1194.

Discher DE, Janmey P, Wang Y-L (2005). Tissue cells feel and respond to the stiffness of their substrate. Science 310, 1139–1143.

Dupin I, Etienne-Manneville S (2011). Nuclear positioning: mechanisms and functions. Int J Biochem Cell Biol 43, 1698–1707.

Eckhart L, Reinisch C, Inoue S, Messner P, Dockal M, Mayer C, Tschachler E (2003). A basement membrane-like matrix formed by cell-released proteins at the medium/air interface supports growth of keratinocytes. Eur J Cell Biol 82, 549–555.

Engler A, Bacakova L, Newman C, Hategan A, Griffin M, Discher D (2004). Substrate compliance vs ligand density in cell on gel responses. Biophys J 86, 617–628.

Fernandez-Gonzalez R, Simoes SDM, Röper J-C, Eaton S, Zallen JA (2009). Myosin II dynamics are regulated by tension in intercalating cells. Dev Cell 17, 736–743.

Ghibaudo M, Saez A, Trichet L, Xayaphoummine A, Browaeys J, Silberzan P, Buguin A, Ladoux B (2008). Traction forces and rigidity sensing regulate cell functions. Soft Matter 4, 1836.

Ghibaudo M, Trichet L, Le Digabel J, Richert A, Hersen P, Ladoux B (2009). Substrate topography induces a crossover from 2D to 3D behavior in fibroblast migration. Biophys J 97, 357–368.

Harris AR, Bellis J, Khalilgharibi N, Wyatt T, Baum B, Kabla AJ, Charras GT (2013). Generating suspended cell monolayers for mechanobiological studies. Nat Protoc 8, 2516–2530.

Harris AR, Peter L, Bellis J, Baum B, Kabla AJ, Charras GT (2012). Characterizing the mechanics of cultured cell monolayers. Proc Natl Acad Sci USA 109, 16449–16454.

Heisenberg C-P, Bellaïche Y (2013). Forces in tissue morphogenesis and patterning. Cell 153, 948–962.

Huh D, Matthews BD, Mammoto A, Montoya-Zavala M, Hsin HY, Ingber DE (2010). Reconstituting organ-level lung functions on a chip. Science 328, 1662–1668.

Inoue S, Reinisch C, Tschachler E, Eckhart L (2005). Ultrastructural characterization of an artificial basement membrane produced by cultured keratinocytes. J Biomed Mater Res A 73, 158–164.

Kandow CE, Georges PC, Janmey PA, Beningo KA (2007). Polyacrylamide hydrogels for cell mechanics: steps toward optimization and alternative uses. Methods Cell Biol 83, 29–46.

Kumar S, Maxwell IZ, Heisterkamp A, Polte TR, Lele TP, Salanga M, Mazur E, Ingber DE (2006). Viscoelastic retraction of single living stress fibers and its impact on cell shape, cytoskeletal organization, and extracellular matrix mechanics. Biophys J 90, 3762–3773.

Last J, Liliensiek S, Nealey P, Murphy C (2009). Determining the mechanical properties of human corneal basement membranes with atomic force microscopy. J Struct Biol 167, 19–24.

Lecuit T, Lenne P-F (2007). Cell surface mechanics and the control of cell shape, tissue patterns and morphogenesis. Nat Rev Mol Cell Biol 8, 633–644.

Lemmon CA, Chen CS, Romer LH (2009). Cell traction forces direct fibronectin matrix assembly. Biophys J 96, 729–738.

Leptin M (2005). Gastrulation movements: the logic and the nuts and bolts. Dev Cell 8, 305–320.

Martin AC, Gelbart M, Fernandez-Gonzalez R, Kaschube M, Wieschaus EF (2010). Integration of contractile forces during tissue invagination. J Cell Biol 188, 735–749.

Maruthamuthu V (2011). Cell-ECM traction force modulates endogenous tension at cell–cell contacts. Proc Natl Acad Sci USA 108, 4708–4713.

Mase GTE, Smelser RE, Mase GTE (2009). Continuum Mechanics for Engineers, 3rd ed., Boca Raton, FL: CRC Press.

McKee CT, Raghunathan VK, Nealey PF, Russell P, Murphy CJ (2011). Topographic modulation of the orientation and shape of cell nuclei and their influence on the measured elastic modulus of epithelial cells. Biophys J 101, 2139–2146.

Mercurieva AA, Birshtein TM (1992). Liquid-crystalline ordering in two-dimensional systems with discrete symmetry. Makromol Chem Theory Simul 1, 205–214.

Mertz AF, Che Y, Banerjee S, Goldstein JM, Rosowski KA, Revilla SF (2013). Cadherin-based intercellular adhesions organize epithelial cell–matrix traction forces. Proc Natl Acad Sci USA 110, 842–847.
Nelson CM, Jean RP, Tan JL, Liu WF, Sniadecki NJ, Spector AA, Chen CS (2005). Emergent patterns of growth controlled by multicellular form and mechanics. Proc Natl Acad Sci USA 102, 11594–11599.
Ng MR, Besser A, Brugge JS, Danuser G (2014). Mapping the dynamics of force transduction at cell-cell junctions of epithelial clusters. Elife 4, e03282.
Notbohm J, Kim JH, Asthagiri AR, Ravichandran G (2012). Three-dimensional analysis of the effect of epidermal growth factor on cell-cell adhesion in epithelial cell clusters. Biophys J 102, 1323–1330.
Owaribe K, Kodama R, Eguchi G (1981). Demonstration of contractility of circumferential actin bundles and its morphogenetic significance in pigmented epithelium in vitro and in vivo. J Cell Biol 90, 507–514.
Pelham RJ (1998). Cell locomotion and focal adhesions are regulated by the mechanical properties of the substrate. Biol Bull 348–350.
Pelham RJ, Wang Y (1997). Cell locomotion and focal adhesions are regulated by substrate flexibility. Proc Natl Acad Sci USA 94, 13661–13665.
Quinlan AMT, Billiar KL (2012). Investigating the role of substrate stiffness in the persistence of valvular interstitial cell activation. J Biomed Mater Res A 100, 2474–2482.
Raghunathan VK, McKee CT, Tocce EJ, Nealey PF, Russell P, Murphy CJ (2013). Nuclear and cellular alignment of primary corneal epithelial cells on topography. J Biomed Mater Res A 101, 1069–1079.
Rauzi M, Lenne P-F, Lecuit T (2010). Planar polarized actomyosin contractile flows control epithelial junction remodelling. Nature 468, 1110–1114.
Rauzi M, Verant P, Lecuit T, Lenne P-F (2008). Nature and anisotropy of cortical forces orienting Drosophila tissue morphogenesis. Nat Cell Biol 10, 1401–1410.
Rees D (2012). Basic Engineering Plasticity: An Introduction with Engineering and Manufacturing Applications, Oxford, UK: Butterworth-Heinemann.
Reinsch S, Gönczy P (1998). Mechanisms of nuclear positioning. J Cell Sci 111, 2283–2295.
Roh-Johnson M, Shemer G (2012). Triggering a cell shape change by exploiting pre-existing actomyosin contractions. Science 335, 1232–1235.
Roure ODu, Saez A, Buguin A, Austin RH, Chavrier P, Silberzan P, Ladoux B (2005). Force mapping in epithelial cell migration. Proc Natl Acad Sci USA 102, 2390–2395.
Solon J, Levental I, Sengupta K, Georges PC, Janmey PA (2007). Fibroblast adaptation and stiffness matching to soft elastic substrates. Biophys J 93, 4453–4461.
Tambe DT, Hardin CC, Angelini TE, Rajendran K, Park CY, Serra-Picamal X, Zhou EH, Zaman MH, Butler JP, Weitz DA, *et al*. (2011). Collective cell guidance by cooperative intercellular forces. Nat Mater 10, 469–475.
Tchao R (1989). Epithelial cell interaction in air-liquid interface culture. In Vitro Cell Dev Biol 25, 460–465.
Tremblay D, Andrzejewski L, Leclerc A, Pelling AE (2013). Actin and microtubules play distinct roles in governing the anisotropic deformation of cell nuclei in response to substrate strain. Cytoskeleton 70, 837–848.
Trepat X, Wasserman MR, Angelini TE, Millet E, Weitz DA, Butler JP, Fredberg JJ (2009). Physical forces during collective cell migration. Nat Phys 5, 426–430.
Trichet L, Le Digabel J, Hawkins RJ, Vedula SRK, Gupta M, Ribrault C, Hersen P, Voituriez R, Ladoux B (2012). Evidence of a large-scale mechanosensing mechanism for cellular adaptation to substrate stiffness. Proc Natl Acad Sci USA 109, 6933–6938.
Tse JR, Engler AJ (2010). Preparation of hydrogel substrates with tunable mechanical properties. Curr Protoc Cell Biol 10, 16.
Vicente-Manzanares M, Ma X, Adelstein RS, Horwitz AR (2009). Non-muscle myosin II takes centre stage in cell adhesion and migration. Nat Rev Mol Cell Biol 10, 778–790.
Vogel V, Sheetz M (2006). Local force and geometry sensing regulate cell functions. Nat Rev Mol Cell Biol 7, 265–275.
Wang YN, Galiotis C, Bader DL (2000). Determination of molecular changes in soft tissues under strain using laser Raman microscopy. J Biomech 33, 483–486.
Wiebe C, Wayne BG, Brodland GW (2005). Tensile properties of embryonic epithelia measured using a novel instrument. J Biomech 38, 2087–2094.
Yeung T, Georges PC, Flanagan LA, Marg B, Ortiz M, Funaki M, Zahir N, Ming W, Weaver V, Janmey Pa (2005). Effects of substrate stiffness on cell morphology, cytoskeletal structure, and adhesion. Cell Motil. Cytoskeleton 60, 24–34.
Yonemura S, Itoh M, Nagafuchi A, Tsukita S (1995). Cell-to-cell adherens junction formation and actin filament organization: similarities and differences between non-polarized fibroblasts and polarized epithelial cells. J Cell Sci 108, 127–142.
Zegers MMP, O'Brien LE, Yu W, Datta A, Mostov KE (2003). Epithelial polarity and tubulogenesis in vitro. Trends Cell Biol 13, 169–176.
Zemel a, Rehfeldt F, Brown AEX, Discher DE, Safran SA (2010). Optimal matrix rigidity for stress-fibre polarization in stem cells. Nat Phys 6, 468–473.